The Astrophysical Journal, 587:806–817, 2003 April 20


# OBSERVATIONAL EVIDENCE FOR MODE COUPLING IN THE CHROMOSPHERIC NETWORK

R. T. James McAteer,[1] Peter T. Gallagher,[1,2] David R. Williams,[1,3] Mihalis Mathioudakis,[1]
D. Shaun Bloomfield,[1] Kenneth J. H. Phillips,[4] and Francis P. Keenan[1]
*Received 2002 June 27; accepted 2002 December 23*

## ABSTRACT

Oscillations in network bright points (NBPs) are studied at a variety of chromospheric heights. In particular, the three-dimensional variation of NBP oscillations is studied using image segmentation and cross-correlation analysis between images taken in light of Ca II $K_3$, H$\alpha$ core, Mg I $b_2$, and Mg I $b_1 - 0.4$ Å. Wavelet analysis is used to isolate wave packets in time and to search for height-dependent time delays that result from upward- or downward-directed traveling waves. In each NBP studied, we find evidence for kink-mode waves (1.3, 1.9 mHz), traveling up through the chromosphere and coupling with sausage-mode waves (2.6, 3.8 mHz). This provides a means for depositing energy in the upper chromosphere. We also find evidence for other upward- and downward-propagating waves in the 1.3–4.6 mHz range. Some oscillations do not correspond to traveling waves, and we attribute these to waves generated in neighboring regions.

*Subject headings:* MHD — Sun: chromosphere — Sun: magnetic fields — Sun: oscillations — Sun: photosphere

*On-line material:* color figure

## 1. INTRODUCTION

It has been well known for many years that magnetic fields in the solar atmosphere play an important role in solar physics (Osterbrock 1961). In the quiet Sun, photospheric magnetic flux concentrations emerge in supergranular interiors and are transported by convection to the cell boundaries to form the so-called network (Schrijver, Hagenaar, & Title 1997; Hagenaar et al. 1999). The chromospheric network is only partially defined in strong chromospheric lines and is brightest at the junctions of several supergranules. These junctions are termed network bright points (NBPs) and show a strong one-to-one spatial correlation with the underlying photospheric magnetic field (Cauzzi, Falchi, & Falciani 2000), leading to the suggestion that these regions are heated by magnetic reconnection events, magnetohydrodynamic (MHD) waves (Rosenthal et al. 2002), or the dissipation of Pedersen electric currents (Goodman 2000). The exact nature of the heating mechanism has been the topic of much discussion. Lou (1995) suggested the plausibility of magnetogravity waves as an extension of the earlier work of Damé, Gouttebroze, & Malherbe (1984) and Kneer & von Uexküll (1993). They found oscillations with frequencies lower than the Brunt-Väisälä cutoff and acoustic cutoff. Further work (e.g., Deubner & Fleck 1990; Bocchialini & Baudin 1995) showed these to be downward-propagating waves. Kalkofen (1997) suggested an alternative theory whereby the low-frequency waves found in the network, typically 1–4 mHz (McAteer et al. 2002, Table 1; Banerjee et al. 2001), are explained by the presence of upwardly propagating MHD waves in the NBPs.

MHD waves are commonly modeled using the thin flux tube approximation. Although this approximation will break down in the upper chromosphere (where the diameter of the flux tube will exceed the pressure scale height), it still provides a good basis for modeling, especially in the network. Hasan et al. (2003) discuss the validity of this approximation up to the mid-chromosphere. In the thin flux tube approximation, a magnetic flux tube in an isothermal atmosphere supports three types of waves (Spruit & Roberts 1983). The pure Alfvén torsional wave is nondispersive and is propagating for any frequency, which negates it as a possible heating mechanism. In a flux tube with a strong magnetic field (as occurs in NBPs), the other types are the transverse, kink-mode wave, and the longitudinal, sausage-mode wave. The corresponding tube speeds are given in Kalkofen (1997) in terms of the acoustic speed, $C_s$ (which is around 9 km s$^{-1}$ in the low chromosphere). Both wave modes are dispersive and propagate at frequencies above their respective cutoffs; otherwise, they are evanescent. The wave will propagate at the appropriate tube speed, followed by a wake oscillating at the corresponding cutoff frequency. The longitudinal cutoff frequency, $\nu_l$, and the transverse cutoff frequency, $\nu_t$, are defined by Kalkofen (1997) in terms of the acoustic cutoff frequency, $\nu_{ac}$ (typically around 5.5 mHz in the chromospheric internetwork $K_{2V}$ bright points; Liu 1974),

$$\nu_l = \nu_{ac}\sqrt{\frac{63 + 48\beta}{60 + 50\beta}}\,, \tag{1}$$

$$\nu_t = \nu_{ac}\sqrt{\frac{1}{2\gamma(1 + 2\beta)}}\,, \tag{2}$$

where $\beta$ is the pressure ratio and $\gamma$ is the ratio of specific heats ($= 5/3$). With a maximum plasma $\beta$ value of 0.5 (Kneer, Hasan, & Kalkofen 1996), this gives a minimum $\nu_t = 2.2$ and $\nu_l = 5.7$ mHz. However, the local conditions (e.g., density, magnetic field) in the network can be quite different from the internetwork such that although $\nu_l$ will not vary by more than 2% from $\nu_{ac}$ (Kalkofen 97), $\nu_t$ may be much lower than 2.2 mHz. The exact value of $\nu_{ac}$ in the magnetized atmosphere may also differ from the internetwork.

[1] Department of Pure and Applied Physics, Queen's University Belfast, Belfast, BT7 1NN, Northern Ireland, UK.
[2] L-3 Communications EER Systems Inc., NASA Goddard Space Flight Center, Greenbelt, MD 20771.
[3] Mullard Space Science Laboratory, Holmbury St. Mary, Dorking, Surrey, RH5 6NT, UK.
[4] NASA Goddard Space Flight Center, Greenbelt, MD 20771.

TABLE 1
DETAILS OF DUNN SOLAR TELESCOPE DATA

| Line | Wavelength (Å) | FWHM (Å) | Instrument | Image Scale (arcsec pixel$^{-1}$) | Formation Height (km) |
|---|---|---|---|---|---|
| Ca II $K_3$ | 3933.7 | 0.30 | Hallé filter | 0.33 | 1800–2000[c] |
| H$\alpha$ | 6562.8 | 0.21[a] | UBF[b] | 0.18 | 1200–1700[c] |
| Mg I $b_2$ | 5172.7 | 0.13[a] | UBF[b] | 0.18 | 700–750[d] |
| Mg I $b_1 - 0.4$ Å | 5183.2 | 0.13[a] | UBF[b] | 0.18 | 200[e] |

[a] Universal birefringent filter; Bonaccini et al. 1989.
[b] Beckers, Dickson, & Joyce 1975.
[c] Vernazza et al. 1981.
[d] Schmieder 1979.
[e] Keller & Koutchmy 1991.

Granular buffeting of network flux tubes at the photosphere can create transverse waves at a frequency above the transverse cutoff that can then propagate up along the field lines in a NBP at the corresponding tube speed. Their speed amplitude will increase because of density stratification, so that when it becomes comparable to the tube speed, they enter the nonlinear range. At this point, mode transformation can occur (Ulmscheider, Zähringer, & Musielak 1991) and the waves can couple (and hence transfer power) to longitudinal waves. This mode coupling occurs preferentially for transverse waves at a frequency, $\nu$, which can transfer most of their power to longitudinal waves at a frequency $2\nu$, with a remnant of power at the original frequency. The interaction is greatest when the two tube speeds are equal; it turns out this speed of maximum interaction is around $0.85C_s$. The longitudinal waves can then shock and heat the surrounding plasma (Zhugzhda, Bromm, & Ulmscheider 1995). Muller & Roudier (1992) and Muller et al. (1994) have discovered that NBPs do possess a rapid, intermittent motion that Choudhuri, Auffret, & Priest (1993) and Choudhuri, Dikpati, & Banerjee (1993) modeled as the creation of transverse mode waves at the photospheric level.

In order to identify such a mechanism in the chromosphere, a number of further tests can be carried out.

Test 1: Power at a frequency $\nu$ in the lower chromosphere should also be identifiable at much reduced power in the upper chromosphere.

Test 2: Power at frequency $2\nu$ should appear in the upper chromosphere.

Test 3: Waves at frequencies above the transverse cutoff should propagate at a speed close to $C_s$.

Test 4: In the upper chromosphere, there may be evidence for waves above the longitudinal cutoff frequency, although to a lesser extent, as they should shock in this region.

Test 5: Oscillations should be quasi-periodic, resulting from the nature of the granular buffeting (Hasan & Kalkofen 1999).

Both longitudinal and transverse traveling waves are observable as intensity changes in carefully chosen wavelength bandpasses. A propagating longitudinal wave results in a periodic compression and, hence, heating of the surrounding plasma. This leads to increased radiation, which is then viewable as a periodic intensity change in the filter bandpass. Transverse waves propagating in a plasma result in a Doppler shift of the line profile of the emitted radiation. This results in a periodic change in intensity in the filtergram as the emitted line profile moves in and out of the chosen bandpass.

In this paper we search for observational evidence of MHD waves by studying intensity changes in NBPs at several wavelengths, corresponding to a range of heights from the photosphere to the upper chromosphere. Section 2 provides a summary of the observations and data analysis. Both fast Fourier transforms (FFTs) and wavelet transforms are used to study NBP oscillations in space and time. The wavelet transforms are also cross-correlated at all frequencies to check for the signature of possible traveling waves. In § 3 we present and discuss the results from each NBP individually and collectively. These results are then further discussed in § 4 in relation to the observational tests mentioned above. Section 5 then summarizes our findings and suggests future extensions of this work.

## 2. OBSERVATIONS

### 2.1. *Data Acquisition*

Observations were carried out on 1998 September 22 with the Richard B. Dunn Solar Telescope (DST) at the National Solar Observatory/Sacramento Peak and were taken as part of an 11 day long joint campaign with the *Transition Region and Coronal Explorer* (*TRACE*) spacecraft. The aim of the campaign was to examine the relationship between quiet-Sun events in the photosphere, chromosphere, and transition region. For this paper Ca II $K_3$, H$\alpha$ core, Mg I $b_2$, and Mg I $b_1 - 0.4$ Å data (DST) were used to provide information as a function of height throughout the chromosphere (Table 1). Figure 1 shows the profile of each filter overplotted on the line profile of the respective wavelength. Both the Ca II $K_3$ and H$\alpha$ core heights of formation were estimated from the VAL model (Vernazza, Avrett, & Loeser 1981). The Mg I $b_2$ core is discussed in Kneer & von Uexküll (1993), who, with a bandpass of 0.6 Å, place it at ~350 km. However, the data presented in this paper have a much smaller bandpass and as such include less of the wings, so they are placed at 700–750 km (Schmieder 1979). Keller & Koutchmy (1991) use data that are 0.4 Å into the red wing of the Mg I $b_1$ line and adopt 200 km as the height of formation. Although our data are 0.4 Å into the blue wing, we also adopt this height of formation.

A 150 minute sequence of $100'' \times 100''$ images were obtained in all wavelengths, centered on a quiet-Sun field (solar_$X = -25''$, solar_$Y = -35''$) with a 45 s cadence. This provided seven NBPs (Fig. 2), four of which (NBPs 1,

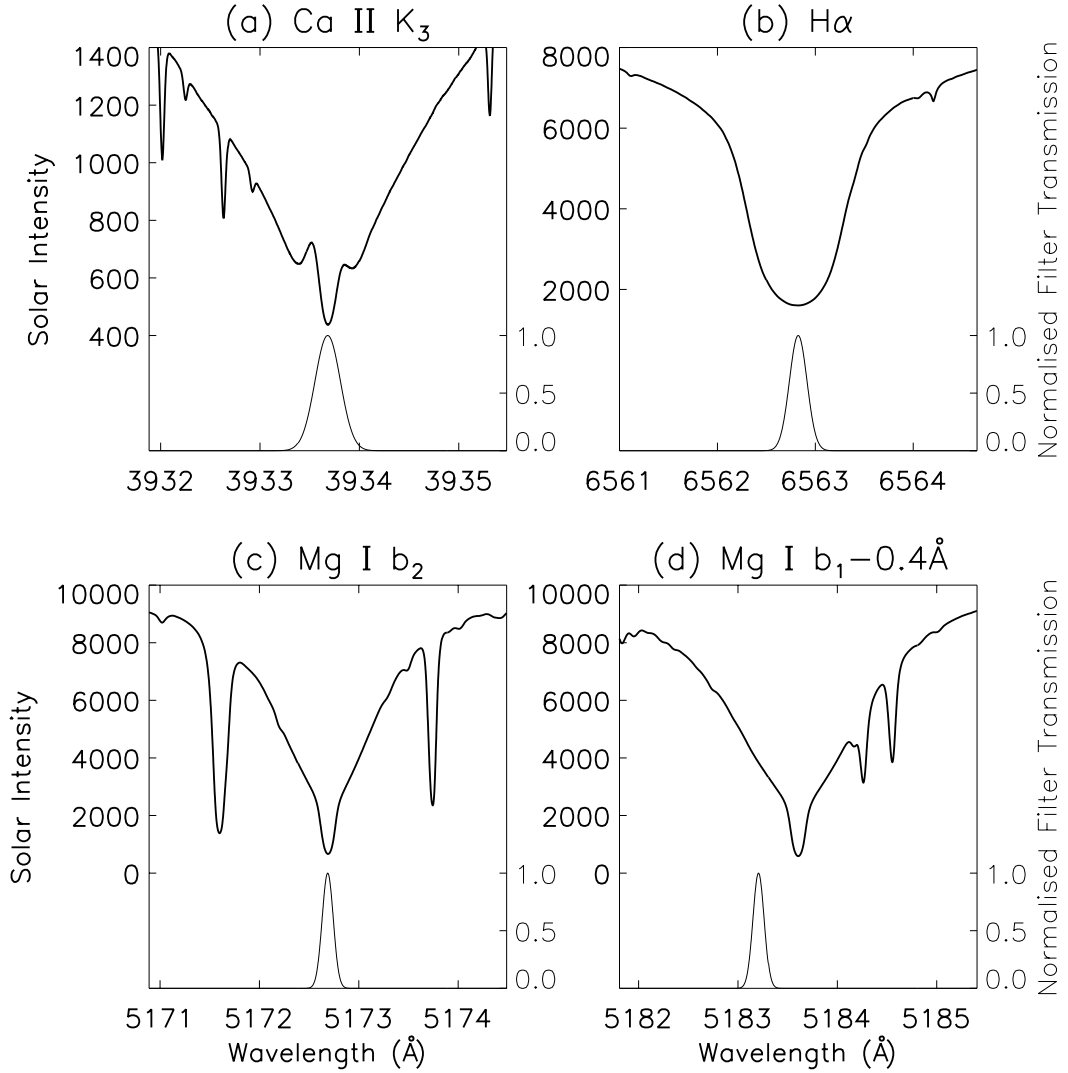


FIG. 1.—Filter profile plotted with line profile for (*a*) Ca II $K_3$, (*b*) H$\alpha$, (*c*) Mg I $b_2$, and (*d*) Mg I $b_1 - 0.4$ Å. In each case, the leftmost *y*-axis is solar intensity, the rightmost *y*-axis is normalized filter transmission, and the *x*-axis is wavelength.

2, 5, and 7) were distinguishable throughout the entire series in all wavelengths and hence are used here. The universal birefringent filter cycle (UBF; Table 1) also included two Fe I (6302.4 Å) images, linearly polarized at 90° to each other. These images were destretched, integrated, and combined to create the magnetogram at the bottom of Figure 2. Co-alignment of the ground-based images with the *TRACE* data led to a calculated spatial size of $0\farcs33$ pixel$^{-1}$ in the Ca II $K_3$ data and $0\farcs18$ pixel$^{-1}$ for the other wavelengths (Table 1). Figure 2 shows that the chromospheric NBPs have a one-to-one spatial correlation with the photospheric magnetic field and exist throughout the transition region, and even into the corona.

### 2.2. *Data Analysis*

Analysis of the DST observations was carried out using standard routines within the *SolarSoftWare* package written in IDL (Freeland & Handy 1998). The data were corrected for CCD readout bias and flat-fielded. Each image was aligned to the first image of the series by means of cross-correlation. *TRACE* images were reduced using the standard calibration and despiking routines provided as part of the *SolarSoftWare* package.

In the case of the ground-based data, the following procedure was also performed. For each NBP, a $30'' \times 30''$ subfield was extracted from which "contrast" light curves were created using the intensity thresholding technique of McAteer et al. (2002). This method calculates the average pixel intensity inside a closed contour, defined by a particular threshold above the modal value of each image in the series, and ensures that only pixels from the NBP itself are included, ignoring any short-lived brightenings (e.g., in the internetwork or supergranular lanes). The resulting light curve is a series of contrast values. The threshold is then increased and the procedure repeated until the threshold value is judged to be at maximum (when less than 10 pixels are contoured). This "thresholding intensity" technique provides information on the spatial evolution of oscillations in NBPs, as the bright center of the NBP is increasingly isolated (McAteer et al. 2002, Figs. 3 and 4). All light curves were then high-pass filtered by convolving them with a suitable Bessel-shaped kernel to remove low-frequency variations. Figure 3 shows the high-pass filter used. This removed all frequencies less than 1 mHz, where slowly varying effects (such as changes in seeing etc.) dominate the spectrum. The filter profile was carefully chosen so as to remove

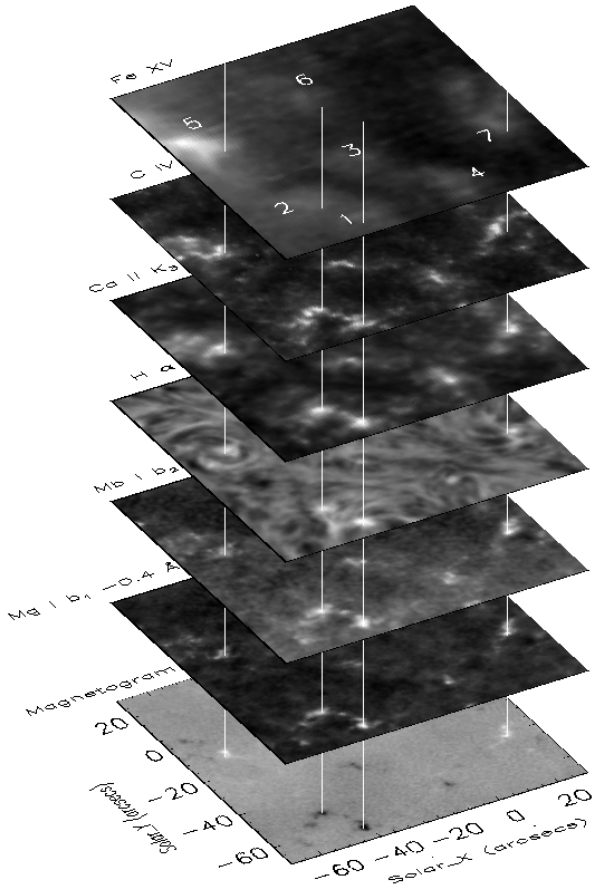


FIG. 2.—Example time-averaged data of the 100″ × 100″ field of view in the corona (EIT 284 Å), transition region (C IV 1500 Å), and chromosphere (DST wavelengths). The bottom plot is the corresponding magnetogram. The vertical lines show the four stable NBPs analyzed in this paper. [*See the electronic edition of the Journal for a color version of the figure.*]

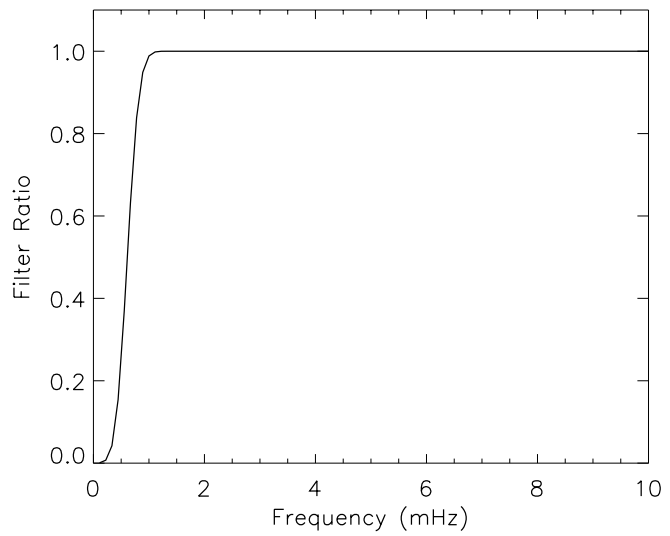


FIG. 3.—Frequency response curve for the high-pass filter used to remove low-frequency variations. Only power under 1 mHz is attenuated.

all this low-frequency power without affecting the rest of the power spectrum (Fig. 4).

As FFTs are unsatisfactory for transient or quasi-periodic signal processing, a wavelet analysis (Torrence & Compo 1998) was also carried out on the maximum threshold light curves using a Morlet wavelet of the form

$$\psi(\eta) = \pi^{-1/4} \exp(i\omega_0\eta) \exp\left(\frac{-\eta^2}{2}\right), \qquad (3)$$

where $\eta = t/s$ is the dimensionless time parameter, $t$ is the time, $s$ is the scale of the wavelet (i.e., its duration), $\omega_0 = s\omega$ is the dimensionless frequency parameter ($\omega_0 = 6$, to satisfy the admissibility condition; Farge 1992), and $\pi^{-1/4}$ is a normalization term. This continuous (and hence nonorthogonal), complex function is ideal for capturing smooth, continous oscillatory behavior but is known to be redundant at large scales (and hence low frequencies), where the wavelet spectrum will be highly correlated (another reason for filtering off low frequencies). Wavelet analysis provides localized temporal and frequency information on the duration and frequency of possible oscillations. Bocchialini & Baudin (1995) noted that although wavelet analysis can be used to obtain phase information, this is very sensitive to frequency. They preferred to determine lags from correlations between their signals, and it is an extension of their method, which is used here. Essentially, from the wavelet power density maps, "power curves" at each frequency were created by taking slices of the wavelet power transform and then cross-correlated to search for time lags (it should also be noted here that the chosen width of the frequency band should be small enough to negate errors arising from the different weighting of each scale; Torrence & Compo 1998). This is now explained in further detail.

For a pair of wavelengths $\lambda_1$ and $\lambda_2$ at a frequency $f$, the power curves $P_{\lambda_1}(f)$ and $P_{\lambda_2}(f)$ were created. The cross-correlation coefficient, $C(\Delta t,f)$, of these power curves as a function of timeshift, $\Delta t$, is given by

$$C(\Delta t,f) = \frac{\sum\left[P_{\lambda_1}(f,t) - \overline{P_{\lambda_1}(f,t)}\right]^2 \times \left[P_{\lambda_2}(f,t+\Delta t) - \overline{P_{\lambda_2}(f,t+\Delta t)}\right]^2}{\left\{\sum\left[P_{\lambda_1}(f,t) - \overline{P_{\lambda_1}(f,t)}\right]^2 \times \sum\left[P_{\lambda_2}(f,t) - \overline{P_{\lambda_2}(f,t)}\right]^2\right\}^{1/2}}. \qquad (4)$$

This is used to evaluate the shift in $P_{\lambda_2}(f)$, which results in maximum correlation. This shift, $\Delta T$, then corresponds to the time lag of $P_{\lambda_2}(f)$ onto $P_{\lambda_1}(f)$ at frequency $f$, and $C(\Delta T,f)$ is an indication of how good the correlation is. This procedure was then repeated for all frequencies and between all pairs of wavelengths. From this time lag information, and from a knowledge of the approximate heights of formation (Table 1), the speed of possible traveling waves at specific frequencies was calculated (Bocchialini & Baudin 1995; Baudin, Bocchialini, & Koutchmy 1996).

## 3. RESULTS

Example wavelet transforms for NBP2 are shown in Figures 5 and 6, where the wavelet diagrams are divided into three boxes. The top panel (*a*) shows the filtered light curve, while the main panel (*b*) shows the wavelet power transform, with frequency as the vertical axis and time along

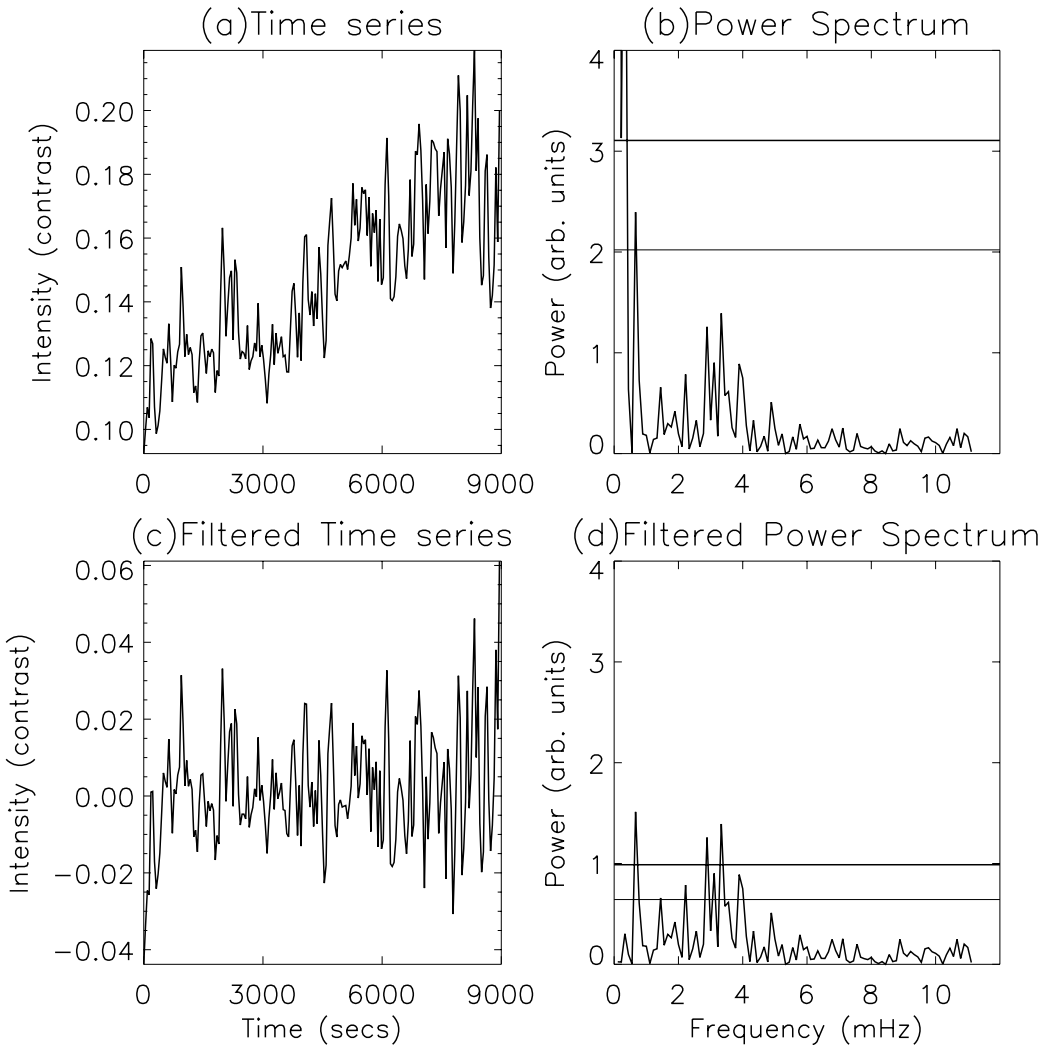


FIG. 4.—Effect of filtering the time series and power spectra of the Ca II $K_3$ light curve for NBP2. The top row (panels *a* and *b*) gives the raw time series and its corresponding power spectrum, while the bottom row (panels *c* and *d*) shows the effects of the low-pass filter. (*a*) and (*c*) share the same *x*-axis, as do (*b*) and (*d*). The thick and thin horizontal lines on the power spectra refer to the 99% and 95% significance levels, respectively.

the horizontal axis. This time axis is the same as in panel (*a*), so that direct comparisons between the occurrence of oscillatory power and the parent time series can be made. The lighter an area, the stronger the oscillatory power. The contours refer to the $\chi^2$-derived 95% confidence level, while the cross-hatched area is known as the cone of influence (COI; Torrence & Compo 1998). Inside this hatched area, edge effects can be significant, so that any power appearing inside the hatched area has to be treated with caution. The right panel (*c*) shows the global wavelet spectrum. This is the sum of power over all time as a function of frequency; as such, it is analogous to the FFT. However, it should be noted that at large wavelet scales (low frequency), peaks will be sharper and hence have a larger amplitude. So it is best to think of the global significance level as a good, but biased, estimate of the true Fourier power. The wavelet transforms clearly show the quasi-periodic nature of the oscillations in all wavelengths (agreeing with test 5), where power at any frequency occurs in the form of wave packets lasting for a few oscillations before disappearing.

Tables 2–9 contain a summary of the behavior of each NBP. Tables 2, 4, 6, and 8 refer to peaks in the FFT power spectrum (and are hereafter referred to as FFT tables). They contain a summary of the behavior of the NBP in each wavelength as a function of thresholding intensity. The "99" and "95" refer to the fact that the power at this frequency reached at least the 99% and 95% confidence levels, respectively. Wavelet diagrams were then used to look at the duration of wave packets at each peak in the FFT. For a frequency to be considered, it must last for at least one full oscillation outside the COI at greater than 95% confidence. Any frequencies that showed more than two complete oscillation periods are marked with a footnote. Together with the FFT confidence level, this gives an indication of the strength and significance of any oscillations. The 200 data points in each light curve and a Nyquist frequency of 11.1 mHz give a frequency resolution of 0.11 mHz. This value is used as the error in the FFT values, and hence all values are grouped in $\pm 0.11$ mHz blocks, with the first value in each column corresponding to the lower limit and the second value corresponding to the upper limit (e.g., the first data column contains any peaks at 1.00, 1.11, and 1.22 mHz).

Tables 3, 5, 7, and 9 contain a summary of the possible traveling waves for each wavelength pair. For every frequency, across every pair of wavelengths the maximum correlation coefficient and corresponding time lag were

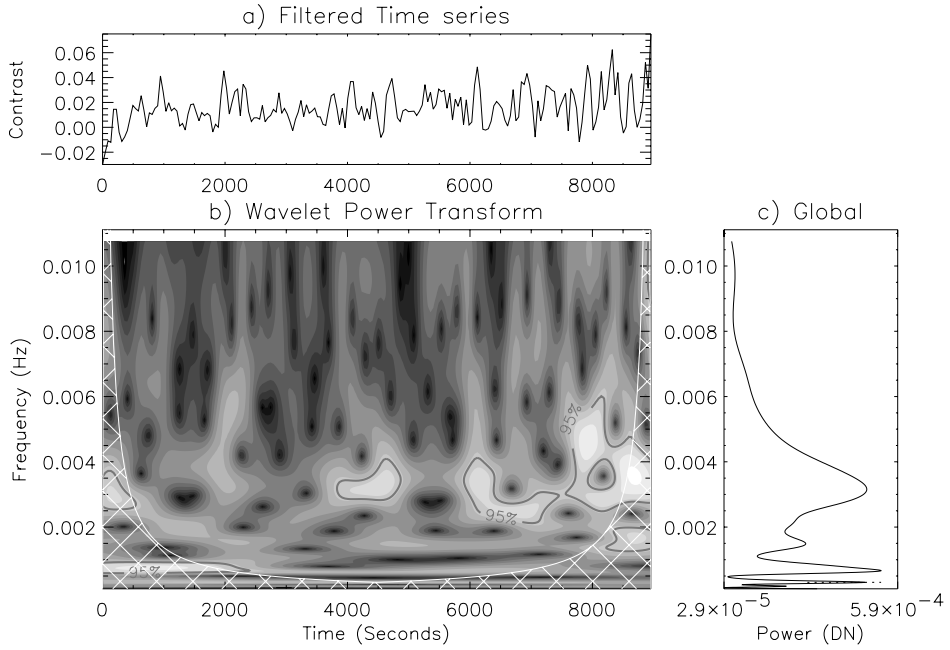


FIG. 5.—(*a*) Filtered light curve from the Ca II $K_3$ data for NBP2. (*b*) Wavelet power transform. The lighter an area, the stronger the oscillatory power. (*c*) The global wavelet spectrum.

recorded. Figure 7 shows the result of this procedure and is now used to explain further steps. In Figure 7*a* there are two peaks in the frequency-correlation curve above 1 mHz: 1.3 mHz (correlation = 0.78) and 1.9 mHz (correlation = 0.68). By drawing horizontal lines from these peaks across into (*b*), the time lag-correlation curve, the corresponding time lags can be obtained. This can also be achieved by drawing vertical lines from these peaks, down into (*c*), the frequency-time lag curve. Maxima in the frequency-correlation curve were retained only if the correlation was above 0.6 and the corresponding time lag was less than 450 s ($10 \times 45$ s cadence). By individual inspection of the power curves, it is clear that correlations of greater than 10 time units could not be attributed to individual wave packets. Any correlations below 1 mHz were also disregarded, as the high-pass filter (Fig. 3) used dictates that there will be no wave packets remaining below this frequency. Wavelet analysis and Fourier transforms were both featureless above 5 mHz, so this is taken as the upper limit to search for correlations. The range of values given in correlation and

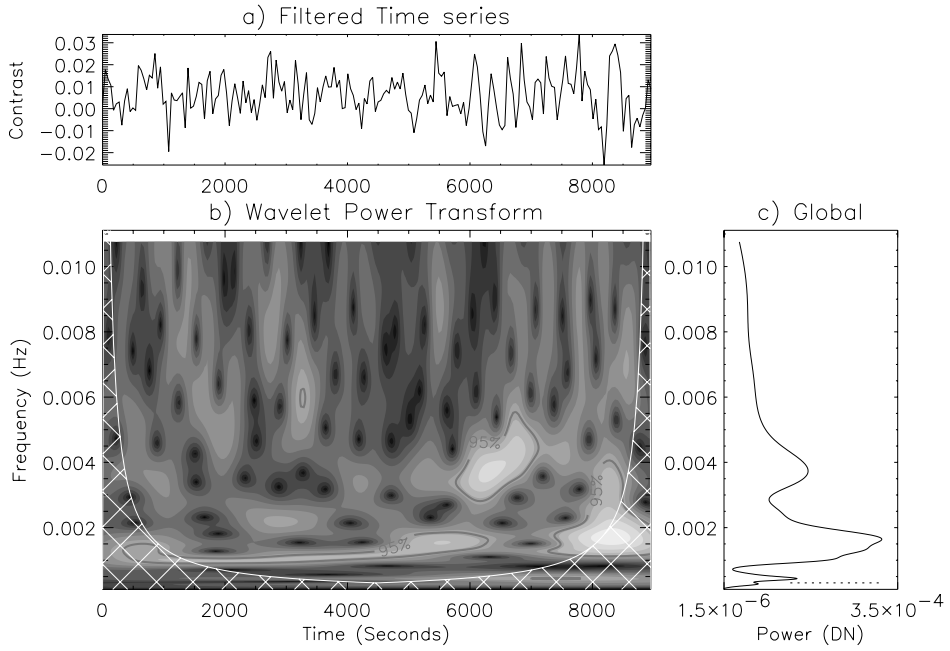


FIG. 6.—(*a*) Filtered light curve from the Mg I $b_2$ data for NBP2. (*b*) Wavelet power transform. The lighter an area, the stronger the oscillatory power. (*c*) The global wavelet spectrum.

TABLE 2

SUMMARY OF FREQUENCIES (mHz) FOR NBP7

| $\lambda$ | 1.00–1.22 | 1.33–1.56 | 1.67–1.89 | 2.00–2.22 | 2.33–2.56 | 2.67–2.89 | 3.00–3.22 | 3.33–3.56 | 3.67–3.89 | 4.00–4.22 | 4.33–4.55 |
|---|---|---|---|---|---|---|---|---|---|---|---|
| Ca II $K_3$ | 99[a] | 95[a] | 99[a] | 99[a] | | | | | | | 95, 95 |
| H$\alpha$ | 99, 99[a] | 99, 95[a] | | 95, 95 | | | | 99[a] | | | |
| Mg I $b_2$ | 99[a] | 99, 95[a] | 99[a], 95 | | | 95 | | 95[a] | 95[a] | | 99[a] |
| Mg I $b_1 - 0.4$ Å | 95, 99 | 95, 95, 95 | 99 | | 95 | | 99 | | | | |

NOTE.— See § 3 for details.

[a] Frequencies that showed more than two complete oscillation periods.

TABLE 3

SUMMARY OF CORRELATIONS FOR NBP7

| $\lambda_1$ | $\lambda_2$ | Correlation Coefficient | Frequency (mHz) | Time Lag (45 s) | Speed (km s$^{-1}$) |
|---|---|---|---|---|---|
| Ca II $K_3$ | Mg I $b_2$ | 0.66–0.72 | 1.5–1.7 | 8–11 | 2–4 |
| Ca II $K_3$ | Mg I $b_1 - 0.4$ Å | 0.81–0.91 | 1.3–1.5 | 0–3 | 12–40+ |
| H$\alpha$ | Mg I $b_2$ | 0.69–0.81 | 1.8–2.0 | 0 to −3 | 3–22+ |
| | | 0.75–0.79 | 2.8–3.0 | −1 to −3 | 3–22 |
| | | 0.83–0.84 | 3.55–3.75 | 4–5 | 2–6 |
| H$\alpha$ | Mg I $b_1 - 0.4$ Å | 0.72–0.81 | 1.8–2.0 | 1–2 | 11–33 |
| Mg I $b_2$ | Mg I $b_1 - 0.4$ Å | 0.96–0.98 | 1.8–2.0 | 1–5 | 2–12 |
| | | 0.69–0.70 | 3.3–3.5 | 2 | 5–6 |

NOTE.— See § 3 for details.

TABLE 4

SUMMARY OF FREQUENCIES (mHz) FOR NBP2

| $\lambda$ | 1.00–1.22 | 1.33–1.56 | 1.67–1.89 | 2.00–2.22 | 2.33–2.56 | 2.67–2.89 | 3.00–3.22 | 3.33–3.56 | 3.67–3.89 | 4.00–4.22 | 4.33–4.55 |
|---|---|---|---|---|---|---|---|---|---|---|---|
| Ca II $K_3$ | | | | | | 99, 95[a] | 99, 95 | 99, 95 | 99[a] | 95[a] | 95[a] |
| H$\alpha$ | 99[a] | 99[a] | | 99[a] | | | | | 95[a] | | 95[a] |
| Mg I $b_2$ | | 99, 99[a] | 99, 95[a] | | | | | 99, 99[a] | | | 95[a] |
| Mg I $b_1 - 0.4$ Å | 95, 99 | 95, 95 | 95, 95 | 95 | | | | | | | |

NOTE.— See § 3 for details.

[a] Frequencies that showed more than two complete oscillation periods.

TABLE 5

SUMMARY OF CORRELATIONS FOR NBP2

| $\lambda_1$ | $\lambda_2$ | Correlation Coefficient | Frequency (mHz) | Time Lag (45 s) | Speed (km s$^{-1}$) |
|---|---|---|---|---|---|
| Ca II $K_3$ | H$\alpha$ | 0.72–0.76 | 2.4–2.6 | 0–4 | 0–17+ |
| Ca II $K_3$ | Mg I $b_2$ | 0.66–0.78 | 1.25–1.45 | 2–4 | 6–14 |
| | | 0.68–0.68 | 1.75–1.95 | 3–8 | 3–10 |
| Ca II $K_3$ | Mg I $b_1 - 0.4$ Å | 0.67–0.78 | 1.2–1.4 | 1–3 | 12–40 |
| | | 0.70–0.73 | 1.7–1.9 | 7–11 | 3–6 |
| H$\alpha$ | Mg I $b_2$ | 0.65–0.67 | 2.97–3.17 | 1–2 | 5–22 |
| | | 0.63–0.65 | 3.85–4.05 | 3 | 3–7 |
| H$\alpha$ | Mg I $b_1 - 0.4$ Å | 0.35–0.57 | 1.15–1.35 | 0 to −13 | 2–33+ |
| | | 0.61–0.62 | 3.2–3.4 | 5 | 4–7 |
| | | 0.62–0.63 | 4.7–4.9 | −2 | 11–16 |
| Mg I $b_2$ | Mg I $b_1 - 0.4$ Å | 0.83–0.93 | 1.3–1.5 | 0–1 | 11+ |
| | | 0.95–0.97 | 1.6–1.8 | 4–6 | 2–3 |
| | | 0.94–0.94 | 4.2–4.4 | −2 | 5–6 |

NOTE.— See § 3 for details.

TABLE 6

SUMMARY OF FREQUENCIES (mHz) FOR NBP5

| $\lambda$ | 1.00–1.22 | 1.33–1.56 | 1.67–1.89 | 2.00–2.22 | 2.33–2.56 | 2.67–2.89 | 3.00–3.22 | 3.33–3.56 | 3.67–3.89 | 4.00–4.22 | 4.33–4.55 |
|---|---|---|---|---|---|---|---|---|---|---|---|
| Ca II $K_3$ ..... | 99, 99, 95 | | | 99[a] | | 95 | | 99[a] | 95[a] | | 95, 95[a] |
| H$\alpha$ ..... | 99, 95[a] | 99[a], 95 | | 99[a] | | 99 | | | 95, 95[a] | 95, 99[a] | |
| Mg I $b_2$ ..... | 99, 99[a] | | | | | 99[a] | 95[a] | 99[a] | | | 99[a] |
| Mg I $b_1 - 0.4$ Å ..... | 99[a] | 99, 95 | | 99[a] | | 95[a] | 99[a] | 95[a] | | | |

NOTE.— See § 3 for details.

[a] Frequencies that showed more than two complete oscillation periods.

TABLE 7

SUMMARY OF CORRELATIONS FOR NBP5

| $\lambda_1$ | $\lambda_2$ | Correlation Coefficient | Frequency (mHz) | Time Lag (45 s) | Speed (km $s^{-1}$) |
|---|---|---|---|---|---|
| Ca II $K_3$ ... | H$\alpha$ | 0.82–0.84 | 3.65–3.85 | −8 to −9 | <2 |
| | | 0.6–0.76 | 3.3–3.5 | 0–1 | 2+ |
| Ca II $K_3$ ... | Mg I $b_2$ | 0.64–0.76 | 0.9–1.1 | −1 to −8 | 3–29 |
| | | 0.56–0.77 | 1.05–1.25 | 0 to −1 | 23+ |
| Ca II $K_3$ ... | Mg I $b_1 - 0.4$ Å | 0.58–0.60 | 4.55–4.75 | −6 to −7 | 5–7 |
| H$\alpha$ ..... | Mg I $b_2$ | 0.55–0.67 | 1.2–1.4 | 0 to −5 | 2–22+ |
| H$\alpha$ ..... | Mg I $b_1 - 0.4$ Å | 0.67–0.68 | 4.15–4.35 | 2 | 11–17 |
| Mg I $b_2$ .... | Mg I $b_1 - 0.4$ Å | 0.80–0.86 | 1.48–1.68 | 0–2 | 6–12+ |
| | | 0.62–0.63 | 4.0–4.2 | −3 | 4 |

NOTE.— See § 3 for details.

TABLE 8

SUMMARY OF FREQUENCIES (mHz) FOR NBP1

| $\lambda$ | 1.00–1.22 | 1.33–1.56 | 1.67–1.89 | 2.00–2.22 | 2.33–2.56 | 2.67–2.89 | 3.00–3.22 | 3.33–3.56 | 3.67–3.89 | 4.00–4.22 |
|---|---|---|---|---|---|---|---|---|---|---|
| Ca II $K_3$ ..... | | | | | | 95 | 99[a] | 99[a] | | 95[a] |
| H$\alpha$ ..... | 99, 95[a] | 99[a] | | 95 | | 99 | | | 99[a] | 99, 95[a] |
| Mg I $b_2$ ..... | 99, 99 | | | | | 99 | 95 | 95 | | |
| Mg I $b_1 - 0.4$ Å ..... | 99 | 99, 95[a] | | 99 | | 95 | 99 | 95 | | |

NOTE.— See § 3 for details.

[a] Frequencies that showed more than two complete oscillation periods.

TABLE 9

SUMMARY OF CORRELATIONS FOR NBP1

| $\lambda_1$ | $\lambda_2$ | Correlation Coefficient | Frequency (mHz) | Time Lag (45 s) | Speed (km $s^{-1}$) |
|---|---|---|---|---|---|
| Ca II $K_3$ ... | H$\alpha$ | 0.66–0.79 | 1.2–1.4 | −3 to −12 | <6 |
| | | 0.61–0.72 | 2.3–2.5 | 4–6 | <4 |
| Ca II $K_3$ ... | Mg I $b_2$ | 0.68–0.75 | 1.9–2.1 | 0 | |
| Ca II $K_3$ ... | Mg I $b_1 - 0.4$ Å | 0.57–0.62 | 1.73–1.93 | 3–7 | 5–13 |
| H$\alpha$ ..... | Mg I $b_2$ | 0.77–0.84 | 1.2–1.4 | −3 to −7 | 1–7 |
| H$\alpha$ ..... | Mg I $b_1 - 0.4$ Å | 0.69 | 4.1–4.3 | 3 | 7–11 |
| Mg I $b_2$ .... | Mg I $b_1 - 0.4$ Å | 0.69–0.79 | 1.5–1.7 | 0–3 | 4–12+ |

NOTE.— See § 3 for details.

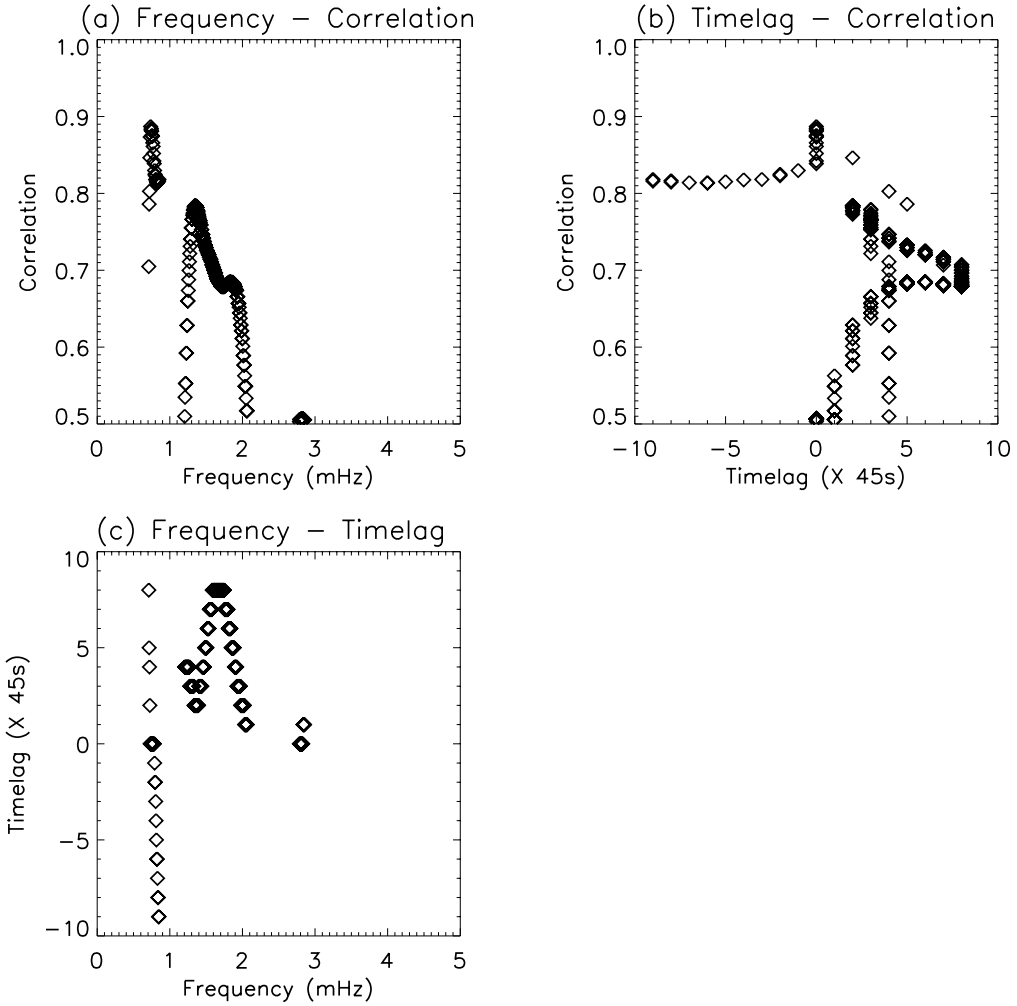


FIG. 7.—Three curves resulting from the correlation of the light curves of NBP2 in Ca II $K_3$ and Mg I $b_2$. (*a*) Peak correlation against frequency. (*b*) Peak correlation against time lag. (*c*) Time lag against frequency. The *x*-axis of (*a*) and (*c*) is the same. The *y*-axis of (*a*) and (*b*) is the same. Hence, the time lag corresponding to the peaks in (*a*) can be determined by drawing horizontal and vertical lines across to (*b*) and down to (*c*), respectively.

time lag is determined by the maximum and minimum correlation and time lag in the frequency range of the chosen frequency ±0.1 mHz. The final column denotes the speed of the wave. It is noted that a data cadence of 45 s, combined with the spread in height estimates (Table 1), leads to a large range of speed estimates. A less than symbol signifies a maximum frequency, whereas a plus symbol signifies that the speed may be faster than the quoted value. It should also be noted here that a negative time lag refers to a downward speed, whereas a zero time lag could suggest either evanescent waves or upward- or downward-propagating waves, within the available time resolution.

Some general comments can be made before concentrating on each NBP individually. In the lower atmosphere (e.g., Mg I $b_1 - 0.4$ Å), the oscillations are concentrated in the bright central portion of each NBP. However, in the upper chromospheric (e.g., Ca II $K_3$), there is a greater tendency for some oscillatory power to exist in the outer regions (i.e., farther from the center of the NBP). This is best demonstrated by moving threshold FFTs (McAteer et al. 2002, Figs. 3 and 4), where the sudden appearance of power at a particular threshold indicates that it is confined in the central portion only. It can be explained in terms of the "magnetic canopy" effect, whereby the magnetic field lines diverge in the upper chromosphere. In the present work, the FFT tables also show a tendency for higher frequency power (~3 mHz) to exist in the upper chromosphere, with lower frequencies (~2 mHz) more powerful in the lower chromosphere. This is in general agreement with test 2. Any power that may occur around 3 mHz in the lower chromosphere is uncorrelated with the upper chromosphere, suggesting that it may be related to the well-known 5 minute photospheric oscillation.

### 3.1. *NBP7: Tables 2 and 3*

Correlations across H$\alpha$, Mg I $b_2$, and Mg I $b_1 - 0.4$ Å show a possible traveling wave at ~1.9 mHz at a speed around $C_s$. The FFTs also reveal a strong peak around this frequency in the lower chromospheric lines, with a weaker peak in H$\alpha$, and the latter also show the appearance of a strong peak around 3.6 mHz. There is also a correlation around 3.6 mHz (H$\alpha$ to Mg I $b_2$) and at 3.5 mHz (Mg I $b_2$ to Mg I $b_1 - 0.4$ Å). This is consistent with tests 1–4, where a transverse wave at 1.9 mHz travels up through the atmosphere and couples to a longitudinal wave at around twice the original frequency when it reaches the height of H$\alpha$ (core) formation temperature. This longitudinal wave then

continues to travel upward and eventually shocks, explaining the lack of power at ~3.5 mHz in Ca II $K_3$. The strong peaks at ~2.0 mHz in Ca II $K_3$ are unexpected but do not appear to be correlated with oscillations at the same frequency in the lower chromosphere.

In the 1.33–1.56 mHz range, the oscillations are initially weak but increase in power in Mg I $b_2$ and H$\alpha$, before decreasing again in Ca II $K_3$. However, there is no power at twice this frequency in Ca II $K_3$, and the only correlation is between Ca II $K_3$ and Mg I $b_1 - 0.4$ Å. There is a downward-moving wave between H$\alpha$ and Mg I $b_2$ (2.9 mHz) and a slow upward-moving wave between Ca II $K_3$ and Mg I $b_2$ (1.6 mHz). Below 1.3 mHz there is significant power in all wavelengths but no indication of any correlation. Several frequencies seem to be localized in height, specifically the peaks around 2.5 mHz in the two lower lines and in the peaks at 4.4 mHz in Mg I $b_2$ and Ca II $K_3$. These may be driven by events spatially removed from the NBP at each height, e.g., granular overshoot (Lites, Rutten, & Kalkofen 1993).

### 3.2. *NBP2: Tables 4 and 5*

Correlations of Ca II $K_3$ to Mg I $b_2$ and Mg I $b_1 - 0.4$ Å, and Mg I $b_2$ to Mg I $b_1 - 0.4$ Å, reveal a possible traveling wave at ~1.4 mHz (also possibly H$\alpha$ to Mg I $b_1 - 0.4$ Å). The FFTs also show power at this frequency, up to the H$\alpha$ level. There is some power at the Ca II $K_3$ level, but it appears inside the COI and hence is not included here. However, Ca II $K_3$ does contain power around 2.8 mHz, and there is some correlation around 2.6 mHz between Ca II $K_3$ and H$\alpha$. This is all consistent with tests 1–4, except for the fact that there is no correlation from H$\alpha$ to Mg I $b_2$. However, this lack of correlation shows the benefit of multiwavelength analysis; although the H$\alpha$-to-Mg I $b_2$ correlation is missing, we can safely rely on correlations across the other wavelengths. It is also worth noting that a transverse frequency of 1.4 mHz, and longitudinal frequency of 2.8 mHz, are low, compared with the suggestions of Kalkofen (1997).

The Ca II $K_3$ to Mg I $b_2$ and Mg I $b_1 - 0.4$ Å correlations, along with that of Mg I $b_2$ to Mg I $b_1 - 0.4$ Å, also show a possible ~1.8 mHz wave. There is some power at this frequency in the lower lines and a weak peak in H$\alpha$ at ~3.8 mHz, with a possible traveling wave at ~3.9 mHz (H$\alpha$ to Mg I $b_2$). However, there is no peak in the higher lying lines at the original frequency. Again, there is some power below 1.3 mHz, with no apparent correlation, and several frequencies seem to be localized in height (e.g., ~3.4 mHz in Mg I $b_2$).

There are several other correlations evident between the lower lines. However, when the frequencies of these correlation peaks are compared with the FFT tables, in many cases there is no associated power in the FFT or wave packets in the wavelet power transforms. This demonstrates the advantage of using wavelet analysis to obtain temporal information and allows us to dismiss the 3.07 mHz (H$\alpha$ to Mg I $b_2$), 3.3, and 4.8 mHz (H$\alpha$ to Mg I $b_1 - 0.4$ Å) correlations. The 4.3 mHz correlation (Mg I $b_2$ to Mg I $b_1 - 0.4$ Å) does correspond to a possible downward-moving wave packet. Waves at around this frequency have been noted before (Bocchialini & Baudin 1995).

### 3.3. *NBP5: Tables 6 and 7*

In the 1.2–1.6 mHz range, there appear to be two different correlation patterns. A ~1.3 mHz correlation (Ca II $K_3$ and H$\alpha$ to Mg I $b_2$) corresponds to a decrease in power (and hence significance) of this frequency in the upper lines. There is also an appearance of signal at ~2.7 mHz in H$\alpha$ and Ca II $K_3$. Although this ~2.7 mHz frequency also occurs in the lower lines, it seems to be uncorrelated to the upper lines. However, there is a lack of correlation between H$\alpha$ and Ca II $K_3$ at ~2.7 mHz (test 4; although this could be due to the longitudinal wave shocking), and the waves may be downward-moving. Also, similar to NBP2, it is of a very low frequency, compared with Kalkofen (1997). An ~1.5 mHz correlation between Mg I $b_2$ and Mg I $b_1 - 0.4$ Å corresponds to a disappearance of power at this frequency from Mg I $b_1 - 0.4$ Å to Mg I $b_2$, as well as the existence of a ~3.1 mHz oscillation in Mg I $b_2$. However, the lack of a remnant peak (test 1) in the upper line makes this a less likely candidate for mode coupling. It would also have coupled too low in the atmosphere to be a viable candidate for chromospheric heating.

The correlation at 4.25 mHz (H$\alpha$ to Mg I $b_1 - 0.4$ Å) corresponds to an appearance at this frequency in H$\alpha$ and could be the indication of a longitudinal wave appearing at this height. There is also power at 2.1 mHz in the lower lines. However, as there is no correlation at 2.1 mHz, and the power at this frequency does not decrease with height, this is not a good candidate for mode coupling. There is a further upward-moving wave at 3.4 mHz (Ca II $K_3$ to H$\alpha$).

There appear to be three downward-moving waves at 1.0 mHz (Ca II $K_3$ to Mg I $b_2$), 3.75 mHz (Ca II $K_3$ to H$\alpha$), and 4.65 mHz (Ca II $K_3$ to Mg I $b_1 - 0.4$ Å), corresponding to wave packets in each wavelength. Bocchialini & Baudin (1995) also found a downward-moving wave at 3.5 mHz using a similar method and invoked the magnetogravity waves suggested by Deubner & Fleck (1990). The 4.1 mHz correlation (Mg I $b_2$ to Mg I $b_1 - 0.4$ Å) does not correspond to any wave packets and is thus dismissed as not being real. Again, there seem to be a few oscillations that are localized in height, mainly in the range 2.67–3.56 mHz in Mg I $b_2$ and Mg I $b_1 - 0.4$ Å. For the frequencies around 3.33 mHz, this could be due to some photospheric leakage. However, as this does not occur in all NBPs, it seems unlikely to be the case.

### 3.4. *NBP1: Tables 8 and 9*

The correlations between Ca II $K_3$ and both Mg I $b_2$ and Mg I $b_1 - 0.4$ Å show a possible traveling wave at ~1.9 mHz (Mg I $b_2$ to Mg I $b_1 - 0.4$ Å also shows a correlation at a slightly lower frequency). This corresponds to an oscillatory signal at ~1.9 mHz in Mg I $b_1 - 0.4$ Å, with reduced power in H$\alpha$. There is also a peak at ~4.0 mHz in H$\alpha$, which is reduced on reaching the Ca II $K_3$ level. H$\alpha$ to Mg I $b_1 - 0.4$ Å shows a traveling wave at ~4.1 mHz (test 4). This all indicates a transverse wave of ~1.9 mHz coupling to a longitudinal wave at ~4.1 mHz, leaving behind a small remnant at the original frequency. This longitudinal wave then shocks, thereby explaining the lack of power in lines produced higher up in the chromosphere.

Again, there is also some weak evidence for downward-moving waves. An ~1.3 mHz correlation is found (Ca II $K_3$ to H$\alpha$ and H$\alpha$ to Mg I $b_2$), although among these three wavelengths an oscillatory signal at this frequency is found in H$\alpha$ only. Hence, the correlation is not necessarily between wave packets. Similarly, the ~2.4 mHz correlation (Ca II $K_3$ to H$\alpha$) does not correspond to any wave packet in either wavelength and hence is dismissed. As in the other cases, a few frequencies exist that do not correspond to any

waves. Below 1.3 mHz there is power up to the H$\alpha$ level. As in NBP5 there is a lot of oscillatory power in the 2.67–3.56 mHz range that does not correspond to any traveling waves.

## 4. DISCUSSION

In each NBP, there is at least one frequency that satisfies the five tests described in § 1. However, a few points must be addressed concerning this. First, Kalkofen (1997) suggests that transverse waves should not normally be viewable at disk center. If they are viewable, it will be due to a flux tube, which, being slightly slanted, will make a small angle with the line of sight. In this case the resulting light curve will have two maxima for each complete oscillation of the wave. However, this will only be true for completely symmetrical profiles. If the line profile is asymmetric, or if the filter is in the wing of the line, the Doppler shift from the transverse wave will result in a light curve that will still contain a signal at the original transverse wave frequency.

Second, the main area of disagreement with theory is in the values of the cutoff frequencies determined from Kalkofen (1997). It should be noted that the cutoffs calculated in § 1 have not been derived specifically for the network. In the network, parameters may vary because of the highly magnetized structure and local depression, which may have an effect on $\nu_t$. A complete understanding of the structure within the network is necessary, which may introduce other factors into the equations given by Kalkofen (1997) for the cutoff frequencies. The results here suggest transverse cutoffs of $\sim$1.3 and $\sim$1.9 mHz, with longitudinal cutoffs at around twice these frequencies. Hasan & Kalkofen (1999) suggest cutoff periods of 534 and 227 s for the longitudinal and transverse mode, respectively, which agree with the higher frequency (1.9 mHz) cutoff suggested here.

Thirdly, results such as those presented here have never before been so clearly demonstrated. It is important to note that our method uses two-dimensional images, making it easier to spatially isolate the NBP throughout the entire time series (as first pointed out by Cauzzi et al. 2000). The contour method also ensures only pixels inside the NBP are included, ignoring any other bright pixels in the field of view. In addition, some oscillatory components can be missed if each NBP is not followed completely from the outer reaches to the bright center. McAteer et al. (2002) also demonstrated how spatially averaging over many NBPs can lead to overlooking power at several frequencies. The "contrast" light curve and digital high-pass filtering techniques used here also remove all very low frequency power, which can dominate the power spectrum (Figs. 3 and 4). It is of course important to remove this low-frequency component without unduly affecting the higher frequencies. It is also of note that the time series used here (150 minutes) is longer than most previous studies. Most importantly, the use of wavelet analysis to create the power curves gives temporal information associated with any wave packets. A Fourier phase analysis, which will average overall time, may result in any correlation across wave packets being "washed out" by the longer nonperiodic component. This may explain the lack of correlation found in this type of analysis (e.g., Lites et al. 1993). It is also important to note the multiwavelength nature of the data used in this study. Although a few papers have previously performed correlations across wavelet power diagrams (Bocchialini & Baudin 1995; Baudin et al. 1996), they have used only two wavelengths in a limited frequency range. Using four wavelengths across all observable frequencies gives a much higher chance of detecting correlated oscillations and makes findings more significant.

Finally, the results reported here suggest longitudinal waves shock in the mid- to high chromosphere, hence heating the surrounding plasma, and the oscillations subsequently disappear. However, simulations by Carlsson & Stein (1992) of K2V grains suggest that these shocks may be coherent, which will lead to further oscillations at 5.5 mHz. This lack of agreement suggests that either the magnetic network differs from the internetwork bright points or the coherence area must be well less than the areas integrated over in this paper.

## 5. CONCLUSIONS

Four individual NBPs have been investigated from their outer region to their bright center using an intensity thresholding technique. Their bright centers are then studied in time using wavelet analysis and throughout the entire chromosphere using correlations at all observable frequencies. For each NBP studied, we have found the possibility of transverse wave propagation in the lower chromosphere. There is also evidence of these transverse waves coupling to longitudinal waves in the upper chromosphere, which can then shock. Thus, mode coupling provides a means of energy transport to heat the upper chromosphere. Each NBP also shows upward- and downward-moving waves in the 1.3–4.6 mHz range. The low cadence of the data makes it difficult to pin down the exact speed of these waves. This uncertainty in speed can be reduced by higher cadence observations and by a better understanding of the height of formation of the wavelengths used, especially in magnetized regions. We have also shown that these NBPs exist into the transition region (Fig. 2), suggesting that although they provide a means of energy transport into the chromosphere via mode coupling, they still exist after the waves have shocked. Further work will involve the study of oscillations in these NBPs into the higher solar atmosphere using simultaneous data in a number of *TRACE* wave bands. An extended study across a much larger number of NBPs in more wavelengths (including high-resolution magnetograms) and, for a longer timespan, will be necessary to confirm these results.

This work was supported by the U.K. Particle Physics and Astronomy Research Council and the Northern Ireland Department of Employment and Learning. J. M. C. A. also thanks Queen's University Belfast for a CAST studentship. D. R. W. also thanks Queen's University Belfast and Rutherford Appleton Laboratory for a CAST studentship. The DST observations were obtained by P. T. G. as a visiting research student at the National Solar Observatory, National Optical Astronomy Observatories, operated by the Association of Universities for Research in Astronomy, Inc. (AURA), under cooperative agreement with the National Science Foundation. We also thank Tom Berger and Ray Smartt for useful advice and discussion regarding data analysis and acquisition. The solar spectrum was obtained from the BASS2000 database.[5] Wavelet software was provided by C. Torrence and G. Compo.[6]

[5] BASS2000 database is available at http://bass2000.obspm.fr/solar_spect.php.

[6] Wavelet software is available at http://paos.colorado.edu/research/wavelets/.

REFERENCES

Banerjee, D., O'Shea, E., Doyle, J. G., & Goossens, M. 2001, A&A, 371, 1137
Baudin, F., Bocchialini, K., & Koutchmy, S. 1996, A&A, 314, L9
Beckers, J. M., Dickson, L., & Joyce, R. S. 1975, A Fully Tunable Lyot-Öhman Filter (Instrumentation Papers 227; Hanscom AFB: Air Force Cambridge Research Lab.)
Bocchialini, K., & Baudin, F. 1995, A&A, 299, 893
Bonaccini, D., Righini, A., Cavalline, F., & Ceppatelli, G. 1989, A&A, 217, 368
Carlsson, M., & Stein, R. 1992, ApJ, 397, L59
Cauzzi, G., Falchi, A., & Falciani, R. 2000, A&A, 357, 1093
Choudhuri, A. R., Auffret, H., & Priest E. R. 1993, Sol. Phys., 143, 49
Choudhuri, A. R., Dikpati, M., & Banerjee, D. 1993, ApJ, 413, 811
Damé, L., Gouttebroze, P., & Malherbe, J.-M. 1984, A&A, 130, 331
Deubner, F.-L., & Fleck, B. 1990, A&A, 228, 506
Farge, M. 1992, Annu. Rev. Fluid Mech., 24, 395
Freeland, S. L., & Handy, B. N. 1998, Sol. Phys., 182, 497
Goodman, L. M. 2000, ApJ, 533, 501
Hagenaar, H. J., Schrijver, C. J., Title, A. M., & Shine, R. A. 1999, ApJ, 511, 932
Hasan, S. S., & Kalkofen, W. 1999, ApJ, 519, 899
Hasan, S. S., Kalkofen, W., van Ballegooijen, A. A., & Ulmschneider, P. 2003, ApJ, 585, 1138
Kalkofen, W. 1997, ApJ, 486, L145
Keller, C. U., & Koutchmy, S. 1991, ApJ, 379, 751
Kneer, F., Hasan, S. S., & Kalkofen, W. 1996, A&A, 305, 660
Kneer, F., & von Uexküll, M. 1993, A&A, 274, 584
Lites, B. W., Rutten, R. J., & Kalkofen, W. 1993, ApJ, 414, 345
Liu, S.-Y. 1974, ApJ, 189, 359
Lou, Y.-Q. 1995, MNRAS, 274, L1
McAteer, R. T. J., Gallagher, P. T., Williams, D. R., Mathioudakis, M., Phillips, K. J. H., & Keenan, F. P. 2002, ApJ, 567, L165
Muller, R., & Roudier, Th. 1992, Sol. Phys., 141, 27
Muller, R., Roudier, Th., Vigneau, J., & Auffret, H. 1994, A&A, 283, 232
Osterbrock, D. E. 1961, ApJ, 134, 347
Rosenthal, C. S., et al. 2002, ApJ, 564, 508
Schmieder, B. 1979, A&A, 74, 273
Schrijver, C. J., Hagenaar, H. J., & Title, A. M. 1997, ApJ, 475, 328
Spruit, H. C., & Roberts, B. 1983, Nature, 304, 401
Torrence, C., & Compo, G. P. 1998, Bull. Am. Meteor. Soc., 79, 61
Ulmschneider, P., Zähringer, K., & Musielak, Z. E. 1991, A&A, 241, 625
Vernazza, J. E., Avrett, E. H., & Loeser, R. 1981, ApJS, 45, 635
Zhugzhda, Y. D., Bromm, V., & Ulmscheider, P. 1995, A&A, 300, 302